A MECHANISM STUDY OF CO-CURRENT AND COUNTER-CURRENT IMBIBITION USING NEW MAGNETIC RESONANCE TECHNIQUES

Quan Chen[a], Karl E. Butler[b], Murray K. Gingras[c], and Bruce J. Balcom[a]

[a]MRI Centre, Department of Physics, [b]Department of Geology, P.O. Box 4400, University of New Brunswick, Fredericton, New Brunswick, E3B 5A3, Canada.
[c]Department of Earth and Atmospheric Sciences, University of Alberta, Edmonton, Alberta, T6G 2E3, Canada.

This paper was prepared for presentation at the International Symposium of the Society of Core Analysts held in Toronto, Canada, 21-25 August 2005

ABSTRACT

When fluid saturated porous media are placed in a uniform magnetic field (B_0) for magnetic resonance (MR) experiments, inhomogeneous internal magnetic fields within the media are generated due to the magnetic susceptibility variations between pore-filling fluid and solid grains. This magnetic field is called the internal field. The magnetic field within each individual pore is heterogeneous, and its spatial variation occurs primarily over the length scale of the pore size. A new MR technique 'Decay due to Diffusion in Internal Field' (DDIF) can be applied to measure the fluid-filled pore-size distribution in porous media. This method detects molecular diffusion of fluid through the internal field in the pore space.

Unlike frequency encoding MRI methods, 'Single-Point Ramped Imaging with T_1 Enhancement' (SPRITE) is largely immune to image distortions generated by susceptibility variations, chemical shift, and paramagnetic impurities. SPRITE enables systems with T_2^* as short as tens of microseconds to be successfully visualized. Our experimental results show that in most sedimentary rocks, a Lorentzian distribution of the internal field arises from susceptibility contrast and a disordered pore structure, which leads to a single exponential T_2^* (effective spin-spin relaxation time) decay which is largely insensitive to fluid saturation in rocks. This suggests that quantitative imaging of local fluid content can be obtained by centric-scan SPRITE technique, since its local image intensity only has T_2^* contrast. However, quantitative imaging may not be achieved by traditional MRI with T_2 (spin-spin relaxation time) contrast, due to multi-exponential T_2 decay in rocks.

Dynamic water imbibition into air-filled rock was studied using DDIF and centric-scan SPRITE techniques. These measurements reveal differences in the pore filling mechanisms for co-current and counter-current imbibition in rock. A piston-like mechanism for co-current imbibition and a film thickening mechanism for counter-current imbibition have been observed.

INTRODUCTION

Spontaneous imbibition is the process by which a wetting fluid is drawn into a porous medium by capillary force. Co-current and counter-current spontaneous imbibition are defined as wetting and non-wetting fluid flow in identical, and opposite directions respectively. Co-current imbibition differs from counter-current imbibition in terms of their dynamic processes and relative permeabilities. In a reservoir, the respective roles played by counter-current imbibition and/or co-current imbibition vary according to the boundary conditions. The imbibition effect is very important for trapped gas in gas reservoirs and oil recovery, especially in fractured reservoirs [1]. Thus, investigation of imbibition has received considerable attention in the literature. Morrow and Mason have recently reviewed developments in this area [2].

Fluid imbibition into capillary tubes, with triangular [3] and square [4] cross-sections, has been studied. Lenormand et al [5] have undertaken fundamental work on the mechanisms of immiscible displacement in capillary micro-model networks with rectangular ducts.

A piston-like front movement for co-current imbibition [6] and more diffuse imbibition fronts for counter-current imbibition [7] have been observed by X-CT in porous media. However, in the absence of direct measurements of pore- and throat- filling processes during spontaneous imbibition in porous media, it has not been possible to prove the suggested co-current imbibition mechanism at the pore-level. Furthermore, the pore-level mechanism of counter-current imbibition in porous media is still unclear.

In the current work, two new magnetic resonance (MR) techniques, i. e., DDIF (Decay due to Diffusion in Internal Field) [8], and Conical-SPRITE imaging [9] are combined to study the mechanisms of spontaneous imbibition in a Berea sandstone [10]. Dynamic spontaneous imbibition processes were monitored by DDIF water-filled pore-size distribution measurements, while the partial 3D water saturation was detected by Conical-SPRITE imaging. Different pore- and throat- filling mechanisms are revealed for co-current imbibition and counter-current imbibition in the Berea sandstone. In addition, we outline some of the basic aspects of the DDIF and MRI measurements and justify the assumptions made in our original analyses [10].

THEORY

DDIF Pore Size Distribution Measurement

When a fluid saturated porous medium is placed in a uniform magnetic field, a spatially varying magnetic field, and its gradients, appear inside the pore space due to susceptibility differences ($\Delta\chi$) between the pore filling fluid and the surrounding solid matrix [11-13]. This susceptibility difference induced magnetic field gradient is called the internal gradient, and it is very strong in sedimentary rocks, compared with experimentally applied magnetic field gradients for NMR diffusion and MRI measurements [14]. The internal magnetic field within a pore is inhomogeneous, and its

spatial variation occurs primary over the length scale of pore size. A recently developed MR technique based on the decay of magnetization due to diffusion in the internal field (DDIF) [9] can be used to determine the pore-size [15] and pore shape [16] in porous media.

The differential equation governing diffusion of longitudinal nuclear spin magnetization is the Torrey-Bloch equation [17]:

$$\frac{\partial}{\partial t} m(\vec{r},t) = D\nabla^2 m(\vec{r},t) - \mu m(\vec{r},t) \tag{1}$$

where, D is the bulk diffusion coefficient, μ is the bulk spin relaxation rate, and m is the deviation of the longitudinal magnetization from its equilibrium value, The acquired signal is $M(t) = \int m(\vec{r},t)dv$.

A solution of the Torrey-Bloch equation can be given in the general form

$$m(r,t) = e^{-\mu t} \sum_{n=0}^{n=\infty} a_n \phi_n(\vec{r}) e^{-t/\tau_n} \tag{2}$$

here ϕ_n and τ_n are eigenfunctions and eigenvalues. The eigenfuctions are normalized over the pore volume V, $(1/V)\int \phi_n^2 dv = 1$. The eigenvalues can be evaluated using the eigenequation:

$$\phi_n / \tau_n = -D\nabla^2 \phi_n(\vec{r}) \tag{3}$$

and the boundary condition at the pore surface:

$$(D\hat{n} \cdot \nabla \phi_n + \rho \phi_n)\big|_s = 0 \tag{4}$$

where $\hat{n}$ is the unit vector normal to the surface (S), and ρ the surface relaxivity.

The eigenmode amplitude a_n, in equation (2) can be determined by the initial condition and the orthogonality of the ϕ_n,

$$a_n = \frac{\int m(r,0)\phi_n(\vec{r})dv}{\int \phi_n^2 dv} \tag{5}$$

The eigenfunctions ϕ_n, and the decay times τ_n for planar geometry with a distance of d between the planes, were derived by Brownstein and Tarr [18]:

$$\phi_n = \cos(\xi_n z / d) \tag{6}$$

$$\tau_n = d^2 / D\xi_n^2 \tag{7}$$

where theξ_n (n=0, 1, 2,…) are the positive roots of the transcendental equation:

$$\xi_n \tan \xi_n = \rho d / D \tag{8}$$

For fast diffusion limit, i.e. $\rho d / D << 1$, the decay time τ_n is given by:

$$\tau_n = d^2 /(Dn^2\pi^2), \quad (n=1,2,3,\ldots) \tag{9}$$

The decay rate of the lowest mode (n=0) is associated with the surface-to-volume ratio (*S/V*) and is approximately $\rho<S/V>$. The higher modes (n>0) are less sensitive to surface relaxivity [19] and diffusive coupling effects between interconnected pores [20] and depend primarily on pore geometry.

The stimulated-echo pulse sequence may be used for DDIF experiment [21]:

$$\frac{\pi}{2} - t_e - \frac{\pi}{2} - t_d - \frac{\pi}{2} - echo \tag{10}$$

The notation π/2 represents a radio-frequency (RF) pulse that rotates the spin vector by an angle of 90 degrees, t_e is the encoding time, while t_d is the diffusion time. The acquired stimulated-echo signal is $E(t_d)$.

This pulse sequence has been extensively employed, in combination with applied pulse field gradients, for diffusion and flow measurements. In the DDIF experiment, no external magnetic field gradient is required.

The first π/2 RF pulse flips the longitudinal magnetization into the transverse plane. The spatially dependent precession frequencies arise from a spatially dependent internal magnetic field distribution $B_z^i(\vec{r})$. After the time t_e, a precession phase difference between spins is given by:

$$\Phi = \gamma B_z^i(\vec{r}) t_e \tag{11}$$

where γ is the gyromagnetic ratio. The second π/2 RF pulse rotates part of the transverse magnetization to the longitudinal direction. A four-step phase cycling for the DDIF sequence was employed [22]. A ± 90-degree phase difference between the first and second RF pulses was chosen, in order to select the sine part of the phase modulation due to the internal field during t_e. Therefore, the magnetization m after the second RF pulse is expressed as:

$$m = m_0 \sin(\Phi) \tag{12}$$

where m_0 is the initial magnetization before the first RF pulse.

After the second π/2 RF pulse, the spatially dependent phase differences are encoded as a spatial pattern of spin magnetization amplitude. The magnetization decay is due to molecular diffusion for a time t_d. A stimulated-echo signal is acquired after the third pulse. The decay of the stimulated-echo arises from the effect of molecular diffusion in the internal magnetic field which varies over the pore space.

In the DDIF experiment, the stimulated-echo signal is acquired for a series of t_d times, to obtain the echo amplitude as a function of t_d. These data are further analyzed to determine a pore size distribution.

A reference pulse sequence is employed to calibrate the effect of spin–lattice relaxation during t_d:

$$\frac{\pi}{2} - t_e - \pi - t_e - \frac{\pi}{2} - t_d - \frac{\pi}{2} - FID \tag{13}$$

where the notation π denotes an RF pulse that rotates the spin vector by an angle of 180-degree. The π pulse is inserted into the DDIF sequence to cancel the phase accumulation due to internal magnetic field, therefore the free induction decay (FID) signal $R(t_d)$, measures only the effect of longitudinal relaxation. An eight-step phase cycle was employed for the reference sequence [22].

When t_e is short, the DDIF modulation is in a weak encoding regime, the range of phase (Φ) variations over the whole sample is less the 2π. Therefore, the modulated spin magnetization reflects the spatial variation of the internal magnetic field. In the weak encoding regime, only the first eigenmode (n=1) is predominately excited, thus under fast diffusion conditions, the pore size d can be determined from the DDIF signal decay rate, by rearranging equation (9) to obtain

$$d = \pi\sqrt{D\tau} \tag{14}$$

The DDIF and reference decay curves for a water saturated Berea sandstone sample are reported in Figure 1. Compared with the reference signal, the fast decay rate of the DDIF data at short t_d arises from molecular diffusion through the internal magnetic field which varies primarily over the pore length scale. At long t_d, when the diffusing molecules have explored all of the spatial variations of the internal magnetic field in the pore space, the decay due to diffusion ceases. At this point, $E(t_d)$ and $R(t_d)$ decay at a similar rate. Thus, the DDIF is a direct reflection of pore geometry. The amplitude of the lowest mode (a_0) can be determined by the ratio of $E(t_d)$ and $R(t_d)$ at a long t_d, and its contribution to $E(t_d)$ can be subtracted. Figure 2 shows that $E(t_d)$-$a_0R(t_d)$ decay as a function of t_d. An inverse Laplace transform was performed with the data of $E(t_d)$-$a_0R(t_d)$ to yield the DDIF spectrum which can be rescaled to yield a pore size distribution with equation (14).

When the porous medium is saturated with water and air, the air may occupy the pores fully or partially. In fully air saturated pores, no NMR signal is generated from those pores. in the partially saturated pores, they are always more water-wet than air-wet. The water spreads on the surface of the pore space, while the air occupies the pore center. The susceptibility (SI unit) values of the experimental samples are: χ[Berea] = 89.85×10^{-6}, χ[water] = -9.05×10^{-6}, χ[air] = 0.36×10^{-6}. As the susceptibility difference between the Berea sandstone and air is similar to the difference between Berea sandstone and water, our investigations [14] have shown that the internal field distributions in the water phase in partially saturated porous media resemble those of a fully saturated sample, DDIF may be employed to explore the water-filled pore size distribution for a partially saturated porous medium.

Conical-SPRITE Imaging

Conical-SPRITE is a 3D version of centric scan SPRITE imaging technique [9], which is a rapid, centric k-space sampling [23], spin-density weighted imaging technique. As a pure phase encoding technique, Conical-SPRITE imaging is largely immune to image

distortions due to chemical shift, susceptibility variations, and other unwanted effects involved with time evolution of the frequency encoding MRI techniques. Compared with the standard SPRITE (single-point ramped imaging with T_1 enhancement) [24] method, Conical-SPRITE has many advantages, such as fast acquisition speed, low duty cycle and reduced sensitivity to longitudinal relaxation time, T_1.

The Conical-SPRITE technique uses a conical k-space trajectory starting from the center of k-space with three ramped phase-encoding gradients. In practice, 39 cones are applied for sampling the 3D k-space cube. The pulse sequence is illustrated in Figure 3. The actual sampling of k-space is discrete, with gradient amplitudes calculated to ensure the sampled points fall on a Cartesian grid. Therefore, a conventional fast Fourier transform can be directly applied for image reconstruction.

For the Conical-SPRITE imaging method, the local imaging intensity (S) is given by:

$$S = M_o \exp(-t_p / T_2^*) \sin\theta \tag{15}$$

where M_o is the equilibrium magnetization, t_p is the phase encoding time, T_2* is the effective transverse relaxation time, and θ is the RF flip angle. Conical-SPRITE is a natural spin density weighted imaging method.

Single Exponential FID in Rocks

A wide range of experimental results [14] show that the overall FID (free induction decay) rate ($1/T_2^*$) in sedimentary rocks is dominated by an internal field distribution (ΔB^i) induced by the large susceptibility difference ($\Delta\chi$) between the pore fluid and solid matrix due to paramagnetic impurities in the solid matrix. The decay rate of the FID and the corresponding NMR linewidth ($\Delta\nu=1/\pi T_2^*$) for fluid saturated sedimentary rocks may be estimated by [14],

$$\frac{1}{\pi T_2^*} = \Delta\nu \approx \frac{\gamma \Delta B^i}{2\pi} = \frac{C\Delta\chi\gamma B_0}{2\pi} \tag{16}$$

where γ is the gyromagnetic ratio, and B_0 is the applied magnetic field strength, while C is a dimensionless constant.

Equation (16) predicts a single exponential T_2* decay, this prediction has been confirmed by a wide range of NMR experiments for sedimentary rocks [14]. We have observed for many sedimentary rocks that T_2* is largely insensitive to water saturation with a single exponential FID. These features ensure that Conical-SPRITE images are essentially spin density images. Spin density images may not be obtained by spin echo based MRI methods, due to multi-exponential T_2 decay in rocks and limitations on the minimum observation time due to the instrument deadtime.

EXPERIMENTS

Berea sandstone samples were employed for the experiments. The porosity was 19%, and permeability 0.2 Darcy. The cylindrical sample for imbibition and NMR experiments was 2.5 cm in diameter and 5.2 cm in length. The cylindrical sample for mercury intrusion was 2.5 cm in diameter and 2.5 cm in length. All experimental samples were extracted from the host rock in close proximity to one another. Furthermore, the samples have a similar pore structure due to the homogeneity of the Berea sandstone. All samples were oven dried at 80 °C until constant mass was reached.

The sample was fully saturated with distilled water under vacuum conditions for DDIF and Conical- SPRITE imaging to determine pore size distribution and porosity distribution. Then, the sample was dried. Spontaneous imbibition experiments were carried out with distilled water. For co-current imbibition, the bottom of the rock sample was kept in contact with a bulk water reservoir. In the case of counter-current imbibition, the whole sample was immersed in a distilled water reservoir. The water was drawn into the center of the core from the surface by capillary forces. At different saturation states, DDIF and Conical-SPRITE imaging experiments were conducted with the sample sealed with Teflon tape to limit evaporation. The sample was repetitively dried, and the procedure repeated several times at different saturation states.

All NMR experiments were carried out in a 2.4 Tesla horizontal bore superconducting magnet (Nalorac Cryogenics Inc., Martinez, CA) with an Apollo console (Tecmag Inc., Houston, TX). The co-current imbibition dynamic process was monitored by 3D Conical-SPRITE imaging with the rock sample and water reservoir inside the magnet, employing a custom made single turn solenoid coil with a vertical orientation and 3.8 cm inner diameter. For all other NMR experiments, a proton-free 4.7 cm inner diameter eight-rung quadrature birdcage probe (Morris Instruments, Ottawa, ON) was employed.

For the DDIF experiments, the t_e was 50 μs, with a series of 35 t_d values chosen to span 10 microseconds to 3 seconds logarithmically. For 3D Conical-SPRITE imaging, the imaging matrix was 64×64×64, the field of view (FOV) was 7 cm ×7 cm ×7 cm, RF flip angle (θ) of 13°, phase encoding time (t_p) of 40 μs, and repetition time (TR) of 2 ms. There were 39 discrete cones sampled for a single scan imaging time which lasted 2.5 minutes.

RESULTS AND DISCUSSION

The pore and throat size distribution and a 3D porosity distribution were obtained with DDIF and mercury porosimetry. Conical-SPRITE imaging was used to determine the sample's imhomogeneity at the pore-level (μm) and at the voxel-level (mm), respectively.

Pore and Throat Size Distribution and Porosity Distribution

An overlay of the DDIF spectrum, for fully water saturated sample, and mercury intrusion results is shown in Figure 4. The amplitudes of the two distributions are scaled to saturation of the mercury and water, respectively. The DDIF spectrum indicates a predominant pore size peak at around 70 μm, which is consistent with the large number of pores with similar diameter observed from the thin-section picture, Figure 5. A shoulder in the distribution extends to a few microns with a reduced amplitude. The throat-size distribution was determined by the mercury intrusion porosimetry measurement. The result shows a single peak at about 15 μm with a very small shoulder down to a few microns. The DDIF and mercury intrusion results indicate that the pore sizes represented by the dominant DDIF peak are interconnected with throat sizes represented by the single peak in the mercury intrusion experiment. The left shoulder of the DDIF spectrum with a size range less than 10 μm, is due to the rough surfaces and lining materials which are shown in Figure 5.

2D longitudinal slice (a) and transverse slice (b) images from 3D Conical-SPRITE image for fully water saturated Berea sandstone core are shown in figure 6. The two slices were selected from the center of the core, a homogenous porosity distribution of the sample was revealed.

Co-Current Imbibition

During co-current imbibition, the DDIF and Conical-SPRITE experiments were combined to monitor the pore-filling processes and 3D saturation evolution, respectively. An overlay of the DDIF spectra for full saturation, and co-current imbibition for 30 minutes with water saturation of 35.5%, as well as co-current imbibition for 13 hours with water saturation of 57.9%, is shown in figure 7. The similar shape of the three DDIF spectra, at different saturation states, indicates that, water flows through the pores and connected throats with a piston-like pattern during co-current imbibition.

The in-situ water content distribution during co-current imbibition is shown with the image series of figure 8. The time interval between successive images was 10.5 minutes. The water signals in the Berea sandstone core show a rectangular shape, and exhibit a piston-like water front movement. Behind the advancing waterfront, no further increase of water saturation was apparent. Water flow with piston-like pattern on the macroscopic scale is due to water filling the pores and connected throats uniformly, which was observed by DDIF experiments on the pore level.

Counter-Current Imbibition

A comparison of the DDIF spectra of full saturation and counter-current imbibition at different saturation is shown in figure 9. The water saturation was 26.3% after imbibition for 8 seconds. At this moment, the DDIF spectrum shows a very low saturation in pores, and relatively higher water saturation in throats in comparison with pores, due to water flow through the pores and throats along the corners and rough surface in the pore space with a film-type structure. Thereby, air must flow along the center of the pores and

throats in the opposite direction. After counter-current imbibition for 84 minutes, the average water saturation was 56.0%. The water saturation did not significantly increase with further imbibition, indicating that water saturation of 56.0% approximately corresponded to the final imbibition equilibrium. The DDIF spectrum still shows a lower saturation in the pores, in comparison with co-current imbibition, due to air bubbles trapped in the center of pores. Trapped gas is directly related and very important to a number of oil and gas recovery processes, such as water invasion into a gas reservoir, water alternating gas (WAG) injection [25] and gas flooding for enhanced oil recovery [26], or oil recovery with pressure below the oil bubble point pressure. The methodologies developed in this paper could be very useful to measure the trapped gas distribution at the pore-level and to understand the trapped gas phenomena and multiphase flow behavior in porous media [27, 28]. This will be useful especially in the routine evaluation of trapped gas by spontaneous imbibition or forced imbibition during relative permeability measurements [29, 30].

Figure 10 shows 2D slices from a 3D Conical-SPRITE image after imbibition for 8 seconds with a bulk water saturation of 26.3%. The water progressed towards, but had not yet reached the center of the sample in these images. A uniform water saturation distribution behind the waterfront is observed. Figure 11 shows 2D slices from a 3D Conical-SPRITE image after imbibition for 15 seconds with a bulk water saturation of 30.9%. The penetrating waterfronts have just merged at the center of the sample. The images reveal a uniform water distribution. Figure 12 shows 2D slices from a 3D Conical-SPRITE image after imbibition for 3 minutes and 53 minutes with bulk water saturations of 45.6% and 51.5%. The two images show a homogeneous distribution with a uniform increase of water saturation.

The Conical-SPRITE image results indicate that water saturation increases globally once the penetrating waterfronts have merged. These results are consistent with a film type penetration mechanism on the pore level as suggested by the DDIF experiments.

For counter-current imbibition, there are two main mechanisms for water saturation evolution, i.e., a water-film front advance mechanism and water-film thickening mechanism. Before waterfronts reach the center of the sample, water flows along the corner and surfaces of the pore network, while air flows along the center of the pore space. After the waterfronts meet and merge at the center part of the sample, water flows continuously with a film-type mechanism, making the pre-existing water-film thicker. This results in a more uniform water distribution with an increase of water saturation during counter-current imbibition.

During counter-current imbibition, the wetting phase (water) and non-wetting phase (air) flow in the same pore-throat channels with opposite direction, resulting in an extra viscous resistance and reduced cross-sectional flow area of each phase for counter-current imbibition compared with co-current imbibition. In counter-current imbibition, the flow of one phase fluid counteracts the flow of the other phase fluid, since the pressure

gradients of the two-phase fluids are oriented in opposite direction. Viscous coupling has a negative effect on counter-current imbibition. In co-current imbibition, the pressure gradients of two-phase fluids are oriented in identical direction. The flow of one-phase fluid has a positive contribution to the displacement of the other phase. Viscous coupling has a positive effect on co-current imbibition [31]. This is especially true in the case of water and oil, which is the reason that counter-current imbibition has a lower imbibition rate, and lower displacement efficiency, under similar boundary conditions [31]. This is mainly due to the viscosity difference of oil and gas.

CONCLUSIONS

This study has combined the DDIF pore size distribution method in partially saturated porous media with Conical-SPRITE imaging to reveal differences in the pore-filling mechanisms for co-current and counter-current imbibition.

During spontaneous co-current imbibition, water displaces air through the pores and connected throats uniformly with a piston-type mechanism. An approximately constant water saturation distribution is observed behind the advancing waterfront.

During counter-current imbibition, water flows through the pores and the connected throats with a film-like pattern, along the corners and the surfaces of the pore space, while air escapes from the sample by flowing through the center of pores and throats in the opposite direction. After the penetrating waterfronts meet at the center part of the core, the pre-existing water film thickens, resulting in a global and uniform increase in water saturation.

ACKNOWLEDGMENTS

BJB thanks NSERC of Canada for operating and equipment grants. BJB also thanks the Canada Chairs program for a Research Chair in MRI of Materials (2002-2009). The UNB MRI Centre is supported by an NSERC Major Facilities Access grant. This research is funded in part by an Atlantic Innovation Fund award to the PanAtlantic Petroleum Systems Consortium, and by Husky Energy, Encana, and Shell Canada. We thank R. MacGregor for his technical assistance.

NOMENCLATURE

DDIF: Decay due to Diffusion in Internal Field;
SPRITE: Single-Point Ramped Imaging with T_1 Enhancement;
T_2*: effective spin-spin relaxation time;
T_2: spin-spin relaxation time;
χ: magnetic susceptibility;
FID: free induction decay;
FOV: field of view.

REFERENCES

[1] Dullien F., *Porous Media: Fluid Transport and Pore Structure*, 2nd ed, Academic, New York (1991).
[2] Morrow N., and G. Mason, *Curr. Opin. Coll. Inter. Sci.* **6**, 321(2001).
[3] G. Mason, and N. R. Morrow, *J. Coll. Inter. Sci.* **141**, 262 (1991).
[4] Dong M. and I. Chatzis, *J. Coll. Inter. Sci.* **172**, 278 (1995).
[5] Lenormand R., C. Zarcone, and A. Sarr, *J. Fluid Mech.* **135**, 337 (1983).
[6] S. Akin, J. M. Schembre, S. K. Bhat, A.R, Kovscek, *J. Pet. Sci. Eng.* **25**, 149 (2000).
[7] Zhou D., L. Jia, J. Kamath and A. Kovscek, *J. Pet. Sci. Eng.* **33**, 61 (2002).
[8] Song Y., S. Ryu, and P. Sen, *Nature (London)*, **406**, 178 (2000).
[9] Halse M., D. Goodyear, B. McMillan, P. Szomolanyi, D. Matheson and B. Balcom, *J. Magn. Reson.*, **165**, 219 (2003).
[10] Chen Q., M. Gingras and B. Balcom, *J. Chem. Phys.* **119**, 9609 (2003).
[11] Brown R. and P. Fantazzini, *Phys. Rev.* B **47**, 14823 (1993).
[12] Borgia G., R. Brown and P. Fantazzini, *Phys. Rev. E* **51**, 2104 (1995).
[13] Hürlimann M., *J. Magn. Reson.* **131**, 232 (1998).
[14] Chen Q., A. Marble, B. Colpitts and B. Balcom, "The internal magnetic field, and single exponential magnetic resonance free induction decay, in rocks", *J. Magn. Reson.* (submitted, 2005).
[15] Y.-Q. Song, *Magn. Reson. Imaging* **19**, 417 (2001).
[16] Chen Q. and Y. Song, *J. Chem. Phys.* **116**, 8247 (2002).
[17] Torrey H., *Phys. Rev.* **104**, 563 (1956).
[18] Brownstein K. and C. Tarr, *Phys. Rev.* A **19**, 2446 (1979).
[19] Song Y., *Phys. Rev. Lett.* **85**, 3878 (2000).
[20] Zielinski L., Y.Song, S. Ryu, and P. N. Sen, *J. Chem. Phys.* **117**, 5361 (2002).
[21] Hahn E., *Phys. Rev.* **80**, 580 (1950).
[22] Song, Y. *Conc. Magn. Reson.* **18**, 97 (2003).
[23] Mastikhin I., B. Balcom, P. Prado and C. Kennedy, *J. Magn. Reson.* **136**, 159 (1999).
[24] Balcom B., R. MacGregor, S. Beyea, D. Green, R. Armstrong, and T. Bremner, J. *Magn. Reson. Series A* **123,** 131 (1996).
[25] Christensen J., Stenby E., abd Skauge A., Review of WAG Field Experience, SPEREE (April 2001) 97-106.
[26] Lake L.: Enhanced Oil Recovery, Prentice Hall, Englewood Cliffs, New Jersey (1989).
[27] Suzanne K., G. Hamon, J. Billiotte, and V. Trocme, " Distribution of trapped gas saturation in heterogeneous sandstone reservoirs", SCA paper 2001-14 in Proceedings of the International Symposium of the Society of Core Analysts, Edinburgh, Scotland, 17-19 September 2001.
[28] Maloney D., and D. Zornes, "Trapped gas versus initial gas saturation trends from a single core test", SCA paper 2003-22 in Proceedings of the International Symposium of the Society of Core Analysts, Pau, France, Sept. 21-24, 2003.

[29] Skauge A., and J. Larsen, "Three-phase relative permeabilities and trapped gas measurements related to WAG processes", SCA paper 9421 in Proceedings of the International Symposium of the Society of Core Analysts, Stavanger, Norway, 12-14 September 1994.
[30] Kralik J., L. Manak, A. Spence, and G. Jerauld, " Trapped gas, relative permeability and residual oil saturation of an oil-wet sandstone", SCA paper 2000-11 in Proceedings of the International Symposium of the Society of Core Analysts, Abu Dhabi, UAE, 18-20 October, 2000.
[31] Bourbiaux B., and F. Kalaydjian, *SPEREE*, 5, 361, (Aug. 1990).

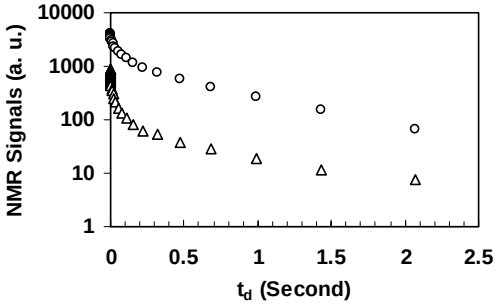

Figure 1. Plot of DDIF signal (Δ), $E(t_d)$, and reference signal (o), $R(t_d)$, as a function of t_d for the Berea sandstone.

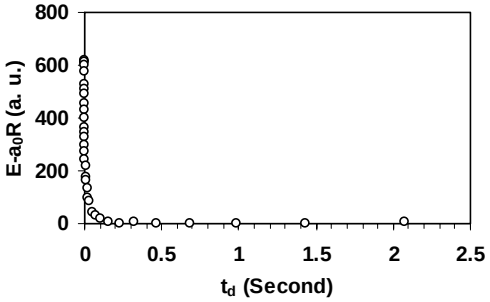

Figure 2. Plot of $E(t_d)$- $a_0R(t_d)$, as a function of t_d. a_0 is determined by the ratio of E to R at long t_d.

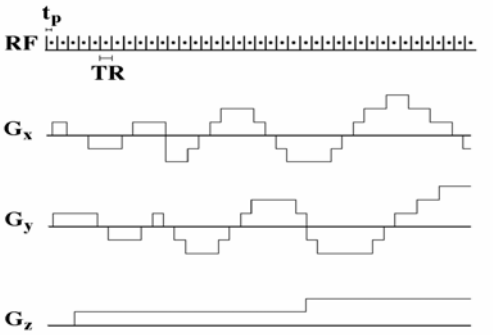

Figure. 3. Conical-SPRITE MRI pulse sequence

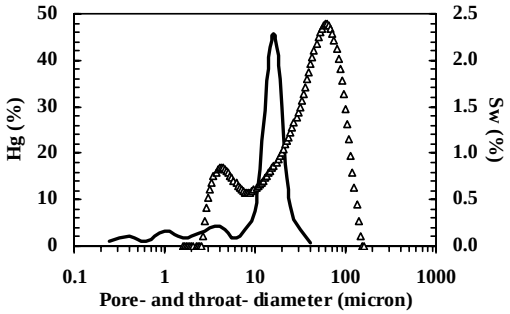

Figure 4. A comparison of pore and throat size distributions for a Berea sandstone sample determined by DDIF spectrum (Δ) and mercury porosimetry (—), respectively.

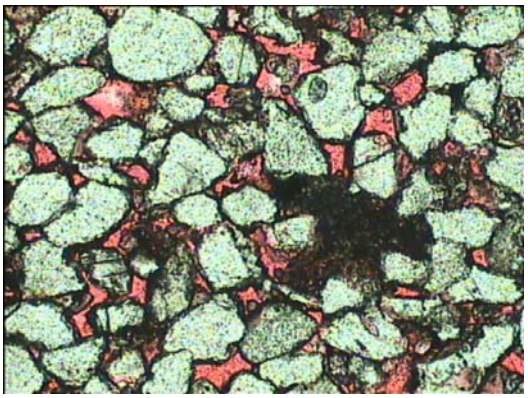

Figure 5. An optical micrograph of a thin-section of the Berea sandstone sample. FOV 1228μm x 921μm. Red dye impregnated resin reveals the pore space.

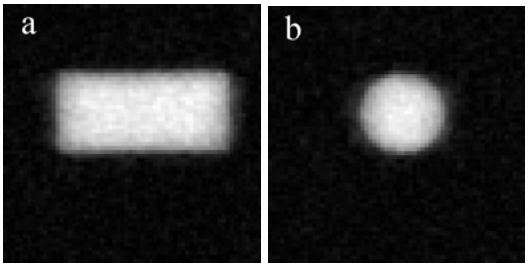

Figure. 6. A 2D longitudinal slice (a), and transverse slice (b), from a 3D Conical-SPRITE image data set for the fully water saturated Berea sandstone.

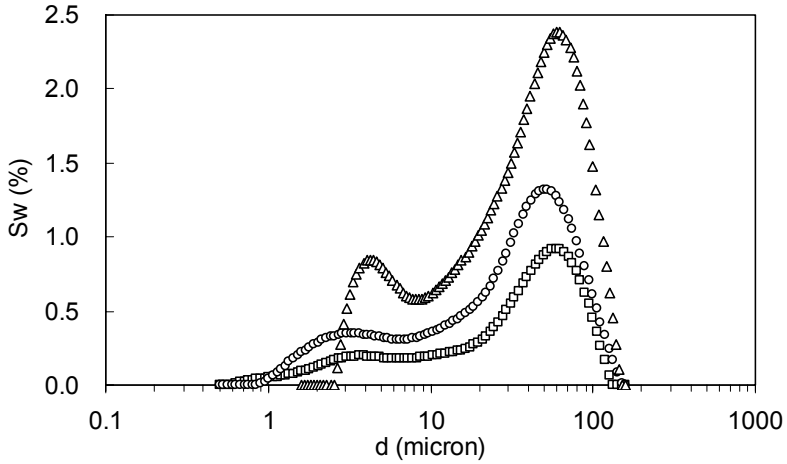

Figure 7. A comparison of the DDIF spectra for fully water saturated (Δ) Berea sandstone, and after co-current imbibition for 30 minutes, with bulk water saturation of 35.5% (□), and after co-current imbibition for 13 hours, with the water saturation of 57.9% (○).

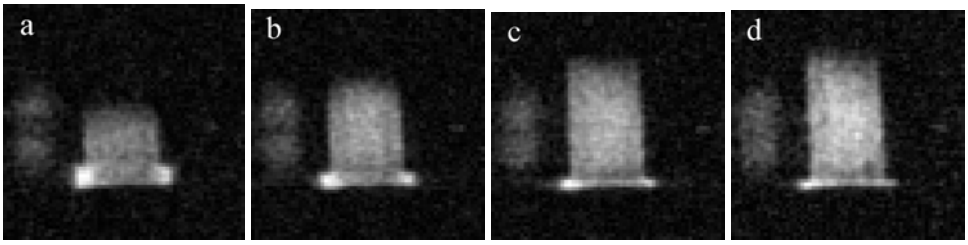

Figure 8. The dynamic process of co-current imbibition for the Berea sandstone observed by Conical-SPRITE imaging. A series of images (a through d) show 2D longitudinal slices from 3D Conical-SPRITE images.

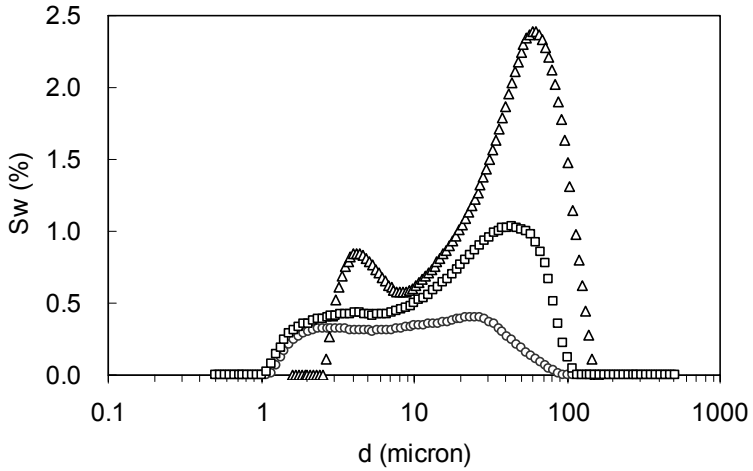

Figure 9. A comparison of the DDIF spectra for fully water saturated (Δ) Berea sandstone, and after imbibition for 8 seconds, the bulk water saturation was 26.3% (○) and after imbibition for 84 minutes with the bulk water saturation of 56.0% (□).

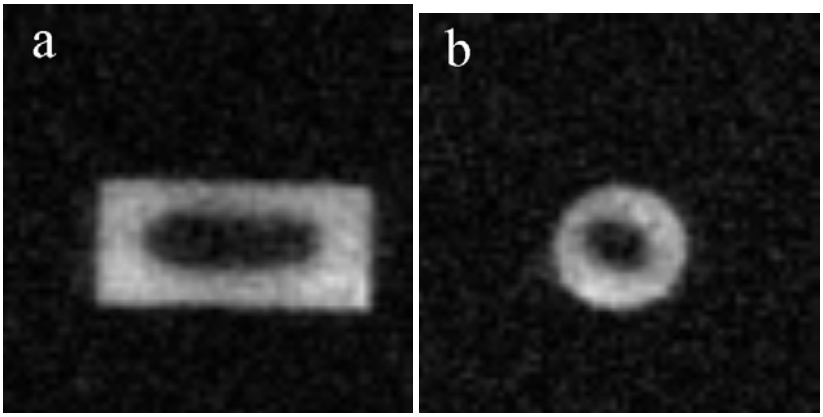

Figure 10. 2D longitudinal (a) and transverse (b) slice from a 3D Conical-SPRITE image, after counter-current imbibition for 8 seconds with bulk water saturation of 26.3%.

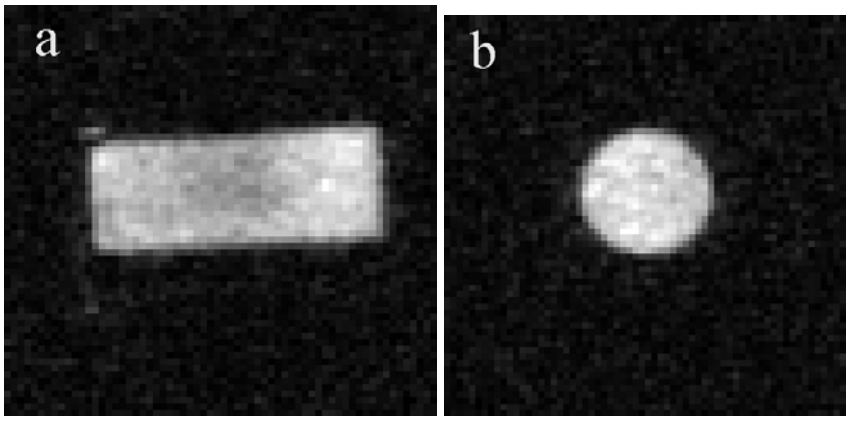

Figure 11. 2D longitudinal slice (a) and transverse (b) slice from a 3D Conical-SPRITE image, after 15 seconds of counter-current imbibition with bulk water saturation of 30.9%.

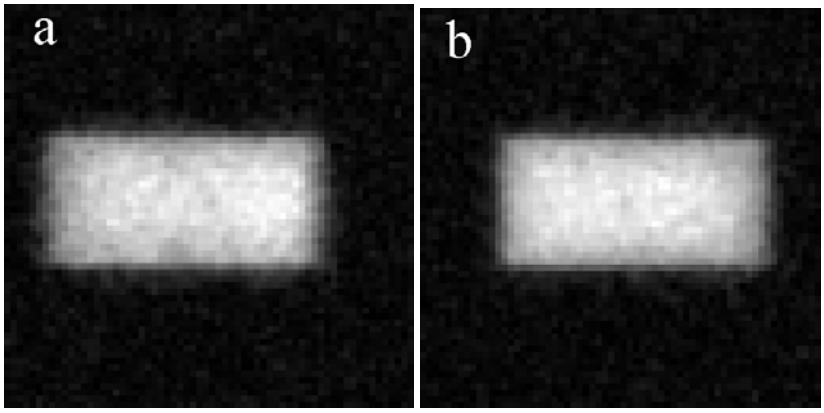

Figure 12. 2D longitudinal slices from two 3D Conical-SPRITE images. (a) After counter-current imbibition for 3 minutes with bulk water saturation of 45.6%. (b) After counter-current imbibition for 53 minutes with bulk water saturation of 51.5%.